Spectroscopy of GaSe Nanoparticle Aggregates

H. Tu, S. Yang, V. Chikan,† and D. F. Kelley*

University of California, Merced, P. O. Box 2039, Merced, California 95344

Received: January 16, 2004; In Final Form: February 12, 2004

The concentration-dependent spectroscopic characteristics of GaSe nanoparticles are interpreted in terms of the particles forming strongly interacting aggregates in high-concentration, room-temperature solutions. The high-concentration absorption spectra are semiquantitatively modeled in terms of the lowest two absorption bands of bulk GaSe, quantum confinement effects, and dipolar coupling between excited state monomers. The model predicts that the lowest energy absorption band shifts slightly to the red and sharpens, while the next band shifts to the blue as the concentration is increased. This correctly explains the observed absorption spectra and their reversible changes with concentrations. Static emission data and initial anisotropies of time-resolved emission may also be qualitatively understood on the basis of this simple model. From the model, the interparticle coupling is estimated to be about -300 cm^{-1}. This is less than the energy differences between adjacent particles in the aggregates but much greater than what is observed between other types of semiconductor nanoparticles. Polydisperse samples have larger energy differences but comparable couplings between adjacent particles. As a result, the spectroscopic effects of aggregation are less pronounced. The nanoparticle aggregate spectra are reminiscent of J-aggregate spectra of organic dyes.

Introduction

Close-packed arrays of colloidal semiconductor nanoparticles typically have spectroscopic properties that are only weakly perturbed from those of well-separated monomers.[1−8] This is because most nanoparticles are covered by an inert layer to passivate the surface. The presence of such a surface passivation layer results in relatively small electronic couplings between adjacent nanoparticles. The largest effect that tightly packing the nanoparticles has on the spectroscopy is a nonspecific one: the adjacent nanoparticles have a different polarizability than the bulk solvent and thereby change the local dielectric environment. This difference in the surrounding media causes small (typically less than 40 cm^{-1}) spectral shifts.[3,9] Although small, there is sufficient coupling to facilitate energy transfer in most cases. This can red shift the emission spectra of the aggregate, compared to the isolated nanoparticles.

In contrast, aggregates of organic dyes can exhibit strong (thousands of wavenumbers) interactions between adjacent dye molecules. These interactions often occur through dipolar coupling and can dramatically change the optical absorption and emission properties of the dye. Organic dyes can form so-called "J-aggregates",[10,11] in which the absorption and emission spectra are red shifted and the spectral profile is considerably altered. The spectroscopy and photophysics of these aggregates have been extensively studied.[12−23] Some of the simplest qualitative features of this spectroscopy may be understood in terms of a very simple case, the dimer.[24] In the simplest case, both monomers are taken to be two-level systems. The lowest excited states of the monomers interact through dipolar coupling and are split into two delocalized states, one at lower and the other at higher energy than the monomer states. When the two monomer transition dipoles are in a head-to-tail geometry, the dimer corresponds to a J-aggregate, and the lower state has all of the oscillator strength. In this case, only the lowest energy state is seen in the absorption and emission spectra. Although common in organic dyes, this type of behavior has not been previously reported for semiconductor nanoparticles.

GaSe nanoparticles have several similarities and differences compared to other types of semiconductor nanoparticles. The most striking differences result from the crystal structure of the bulk GaSe. Specifically, bulk GaSe has a layered crystal structure, consisting of Se−Ga−Ga−Se tetralayer sheets.[25] The Se atoms form hexagonal close packed planes, defining the *x*,*y*-plane of the material. Gallium atom dimers are aligned perpendicular to the *x*,*y*-plane (defining the *z*-axis) in the trigonal prismatic sites between the top and bottom selenium atom planes. The tetralayer sheets are comparatively weakly bound to each other. Because of this unusual crystal structure, GaSe forms two-dimensional nanoparticles that consist of single tetralayer sheets; they are exactly four atoms thick.[26] Since all of the nanoparticles have the same thickness, the extent of *z*-axis quantum confinement is the same for all of the particles. However, the *x*,*y* dimensions can be varied and these nanoparticles have spectroscopic properties that are size dependent.

We have recently begun to study the size-dependent spectroscopy and relaxation dynamics of GaSe nanoparticles.[26−29] We have shown that the spectroscopy of these particles can be understood in terms of the extents of *x*,*y*- and *z*-quantum confinement of the electron−hole pair. Our initial studies used polarized time-resolved and static emission spectroscopy to partially elucidate the ordering of energy levels and the electron and hole relaxation and trapping dynamics. We were able to show that, in the nanoparticles, the lowest energy absorption and emission oscillators are aligned perpendicular to the nanoparticle *x*,*y*-plane, just as in the case of bulk GaSe. Time-resolved results showed that the emission is depolarized by hole

* To whom correspondence should be addressed. E-mail: dfkelley@ucmerced.edu.

† Present address: Division of Chemical Sciences, Lawrence Berkeley National Laboratory, 1 Cyclotron Road, Mail Stop 2R0300, Berkeley, CA 94720.

10.1021/jp049764h CCC: $27.50
Published on Web 03/19/2004

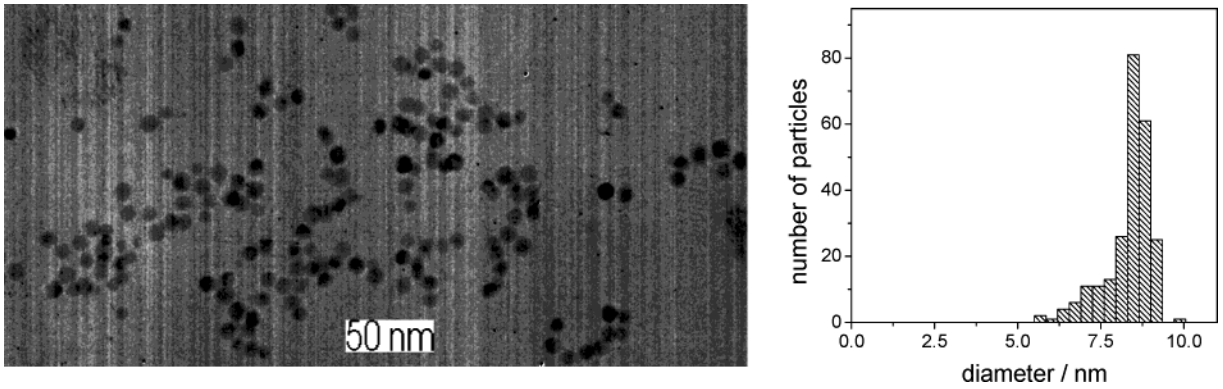

Figure 1. (A, left) TEM image of the monodisperse nanoparticles used in these studies. (B, right) Histogram of the particle diameters measured in the TEM images (this includes the particles in part A) and in other images.

trapping. Further studies used transient absorption polarization spectroscopy to assign the electron and hole intraband transitions.[29]

In this paper we show that GaSe nanoparticles can form aggregates with comparatively strong interactions between the monomers. We find that the two-dimensional nature of these nanoparticles results in aggregation properties that are unprecedented among semiconductor nanoparticles. We show that these spectra can be semiquantitatively understood in terms of a simple dipolar coupling model and that much of the aggregate spectroscopy is reminiscent of that of J-aggregates of organic dyes. The results presented here elucidate some of the basic spectroscopy of the aggregates.

Experimental Section

1. Measurements. Time-resolved emission results are obtained by time-correlated single photon counting. In the 360−444 nm range, the sample is excited with approximately 10 nJ, 150 fs pulses from the second harmonic of a Ti:sapphire laser (Coherent Mira 900F) that is cavity dumped at a repetition rate of 2 MHz. In the 292−315 nm range, the sample is excited with approximately 1 nJ, 7 ps pulses from the second harmonic of a synch-pumped dye laser (Spectra-Physics 3500) that is cavity dumped at a repetition rate of 4 MHz. In both cases the excitation spot sizes are about 1 mm. Decreasing the excitation intensity by a factor of 3 has no effect on the observed emission kinetics. Detection is accomplished with a Hamamatsu 6 μ MCP PMT and time-correlated single photon counting electronics (EG&G Ortec). Wavelength selection is accomplished using a 0.25 m monochromator with a 150 groove/mm grating. The instrument response function is determined by observing the laser scatter, and is about 35 ps fwhm. Polarized emission detection is accomplished using a Polaroid emission polarizer in a near collinear geometry.

Static emission spectra are obtained with a Jobin-Yvon Fluorolog 3. This instrument uses a double excitation monochromator and a 0.32 m detection spectrograph, with a CCD detector. The spectra reported here were obtained with a 300 groove/mm grating, blazed for 450 nm in the detection spectrograph. Emission spectra are not corrected for instrument response; however, the instrument response is fairly flat over the region of the study. The excitation lamp function was determined using coumarin dyes. Absorption spectra were obtained using a Hewlett-Packard 5486 diode array spectrophotometer. TEM (transmission electron microscopy) results were obtained at the National Center for Electron Microscopy at Lawrence Berkeley Labs, using a TopCon microscope, operating at 160 keV.

2. Sample Preparation. GaSe nanoparticle samples are synthesized using variations of the same methods as reported in previous publications.[26−29] The particle size distribution is controlled by varying the reactant concentrations as particle growth occurs. This can result in "focusing" or "defocusing" of the size distribution, much as is done in the case of CdSe nanoparticles.[30] The first step in this synthesis is the preparation of a dried and degassed solution of trioctylphosphine selenium (TOPSe), made from 12.5 mL of trioctylphosphine (TOP) with 1.579 g of Se (99.999%). This solution is added to a solution of 15 g of trioctylphosphine oxide (TOPO) and 5 mL of distilled TOP. The above TOP/TOPO/TOPSe reaction mixture is heated to 280 °C. This is followed by the fast injection of 0.8 mL of $GaMe_3$ dissolved in 7.5 mL of distilled TOP. Upon injection, the temperature drops about 30 °C, and is maintained at 268 °C thereafter. The reaction is allowed to proceed for about 40 min, and an optically clear solution of GaSe nanoparticles having average diameters of 5 nm is obtained. To obtain larger nanoparticles and to control the size distribution, three subsequent procedures can be used and are discussed below.

In the first method, the reaction mixture containing the 5 nm particles is rapidly cooled to about 40 °C. At this point a portion of the sample is removed (to keep the total volume close to constant) and an aliquot $GaMe_3$/Se/TOP solution (0.7 mL of $GaMe_3$ and 0.7 g of Se dissolved in 15 mL of TOP) is added to the sample. The sample is then reheated to 300 °C. Reheating takes about 30 min. The temperature is maintained at 300 °C for about 5 min and then is rapidly recooled to 40 °C. This procedure of cool−inject−heat is repeated four times and then rapidly cooled, resulting in the absorption spectra of the toluene-diluted samples showing progressively less absorbance in the 350−390 nm region and a more pronounced 410−440 nm shoulder. TEM images of these samples are shown in Figure 1A. A histogram of the size distribution may be derived from these images and is presented in Figure 1B. These images indicate that the average size of these nanoparticles is about 8.4 nm, and that the size distribution has a standard deviation of about 8%. Much of the dispersion comes from the small diameter tail of the distribution. If the smallest 9% of the particles are excluded, the standard deviation drops to about 5%. We note that preparation of the TEM grid may selectively deposit the smallest particles, and the actual size sample in solution may be more monodisperse than indicated by the TEM results. These are the most monodisperse samples that we have synthesized, and it is these nanoparticles that are used in the results presented here, unless indicated otherwise. An absorption spectrum of a toluene-diluted sample produced by this method is shown in Figure 2.

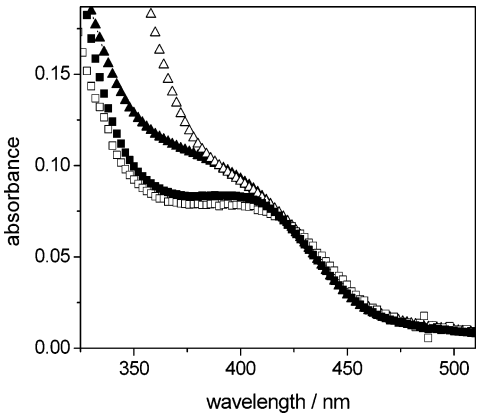

Figure 2. Absorption spectra of dilute samples of GaSe nanoparticles in toluene. The spectra of the monodisperse (solid squares), slightly polydisperse (open squares), very polydisperse (open triangles), and size selectively precipitated (solid triangles) samples are shown. The spectra have been scaled to give the same absorbance at 420 nm.

The following variation of this procedure results in a slightly broader absorption onset and therefore a slightly more polydisperse sample. By use of the same procedure as that described above, nanoparticles having diameters of 5 nm are initially grown. The temperature is maintained at 268 °C and another $GaMe_3$/TOP solution (1.2 mL of $GaMe_3$ dissolved in 12.5 mL of TOP) is periodically injected into the reaction mixture in much smaller aliquots (0.1 mL) over a total reaction time of about 3 h. During the final hour of the reaction, in addition to the $GaMe_3$ injections, a TOPSe solution (0.8 g of Se dissolved in 5 mL of distilled TOP) is also periodically injected into the reaction mixture in 0.1 mL aliquots. This is the procedure that we have used to produce particles for our previous studies.[29] TEM images indicate that the average size of these nanoparticles is about 9 nm, and that the size distribution is about ±10%. An absorption spectrum of this sample diluted in toluene is also presented in Figure 2.

Other procedures can also be used to manipulate the size distribution. If the reaction is allowed to proceed for several hours without the addition of more reactants, Oswald ripening broadens the nanoparticle size distribution. This results in a very polydisperse sample. Figure 2 shows an absorption spectrum of such a sample, diluted in toluene. We note that the size distribution of a polydisperse sample may be narrowed by size-selective precipitation. Dilution with any alkane (typically octane) will result in precipitation of the smallest particles and therefore a turbid solution. This solution may be centrifuged to give a clear solution, whose absorption spectrum is also shown in Figure 2.

In a previous publication we used TEM imaging to establish a relationship between the particle size and the inflection point in the onset of the absorption spectrum.[29] The wavelength of the inflection point is given by

$$\lambda = 10^7 R^2/(22420R^2 + 5817) \qquad (1)$$

where R is the radius of the nanoparticles in nanometers and λ is the inflection point in nanometers. (The constants in this equation have been very slightly refined since our original publication.[29]) Later, we show that the center of the inhomogeneously broadened lowest transition is about 2000 cm^{-1} to the blue of the inflection wavelength. From this equation, we find that the monodisperse sample (synthesized by the first method described above) and the slightly polydisperse sample (synthesized by the second method) both have average diameters of 8−9 nm. The polydisperse sample synthesized by an extended reaction has an average diameter of about 7 nm. This sample exhibits considerably more absorbance in the 360−400 nm region, which may be assigned to smaller particles, in the 4−6 nm range. Following size-selective precipitation, this sample has far less absorption in the 360−400 nm range, indicating that many of the 4−6 nm particles have been removed. As a result, the absorption inflection point moves slightly (about 1 nm) to the red. Consistent with these results, octane dilution of the samples produced by the first method (having the smallest size dispersion and the fewest small particles) results in little or no precipitation.

All of these samples have a total gallium concentration on the order of 0.3 M. The 9 nm particles have roughly 1000 gallium atoms per particle, so these solutions have nanoparticle concentrations of about 0.3 mM. For convenience in later discussion, the three samples synthesized by the first, second, and third methods are referred to as monodisperse, slightly polydisperse, and polydisperse samples, respectively. No further results on the size selectively precipitated sample will be presented.

This paper assigns spectroscopic features to nanoparticle aggregates and infers aggregate structure from spectroscopic measurements. An obvious complementary experiment is to attempt to obtain TEM images of these aggregates. Indeed, we have obtained many TEM images of these particles and often see regions where the particles are aggregated on the TEM grid. However, simple energetic considerations suggest that aggregates seen on a TEM grid may not bear any structural resemblance to the aggregates present in solution. If the solution phase aggregates are assumed to have a stacked geometry (spectroscopic evidence indicating that this is the case is presented below), interaction between the monomers occurs at the top and bottom surfaces. These surfaces are coordinately saturated, and the solution phase aggregates are held together only by van der Waals forces. This is consistent with the rapid formation and dissolution of the aggregates upon solution concentration or dilution. The nanoparticles will also have comparable van der Waals interactions with the TEM grid. Thus, the presence of the TEM grid is expected to greatly perturb the nanoparticle aggregates. Due to this consideration, we do not believe it is possible to interpret the spectroscopy of solution phase aggregates in terms of images of aggregates on a TEM grid, and these images will not be presented or further discussed.

Results and Discussion

1. Assignment of Aggregate Spectral Features. Concentration-dependent absorption spectra of monodisperse GaSe nanoparticles diluted with toluene are shown in Figure 3. The most obvious change in the absorption spectrum is that a resolved peak is formed at the highest concentrations. This is primarily because there is a significant relative loss of absorption in the 300−360 nm region. Specifically, the 400 nm absorption increases slightly supralinearly with concentration and the 300−350 nm absorption increases quite sublinearly with concentration. Careful inspection of Figure 3 also reveals that the red edge absorption onset is slightly sharper and very slightly red shifted in the case of the high concentration samples. The spectral changes that occur upon diluting a concentrated sample are reversible; pumping off the solvent results in almost complete recovery of the original spectrum. These spectroscopic characteristics have not been previously reported for any other type of colloidal semiconductor nanoparticles.

There are three obvious possibilities for the assignment of the spectral changes:

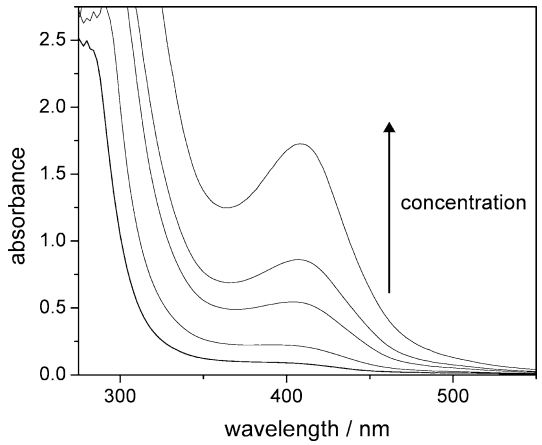

Figure 3. Concentration-dependent absorption spectra of the monodisperse sample. The concentrations range from no dilution (the concentrated solution in the TOP/TOPO reaction mixture) to diluted by a factor of 20 in toluene.

1. They are due to specific nanoparticle−solvent interactions; for example, formation of a charge transfer band upon solvent addition.

2. They are due to nonspecific dilution effects, that is, caused by changes in the individual nanoparticles. Specifically, the spectroscopic changes could be assigned to changes in the nanoparticle size distribution.

3. They are due to aggregation of the nanoparticles.

We will consider each of these possibilities. Possible assignment 1 is eliminated by the observation that the same effects are observed for dilution with very different types of solvents. We find that the nature of the solvent affects particle surface chemistry and therefore the carrier relaxation (trapping) dynamics. (Exciton dynamics in these aggregates will be discussed in a later paper.) However, nearly identical absorption spectra are observed when the particles are diluted in butanol, toluene, octane, pyridine, or a constant composition TOP/TOPO mixture. If the spectral changes were due to specific nanoparticle/solvent interactions, different spectra would be expected in different solvents. Possible assignment 2 suggests that the sizes of the particles are controlled by the concentration; i.e., the size distribution is controlled by thermodynamics. Such an assignment is not unprecedented. Thermodynamic control of particle size distributions have been observed in several types of nanoparticles (gold, MoS_2),[31−33] and it is known that thermodynamics plays a central role in determining the size distribution during the growth of the particles,[29] similar to what is observed in the case of CdSe nanoparticles.[30] However, two observations indicate that, in the case of GaSe nanoparticles, the final size distribution is not controlled by postsynthesis (room temperature) thermodynamic considerations. This is equivalent to saying that the particles are not labile at room temperature. First, we have imaged different sizes of particles, ranging from 2.5 to 9 nm.[26,29] In all cases the TEM grids are prepared by first diluting the samples to very low concentrations in hexane or octane. Different sizes of particles are observed in the TEM images, consistent with the different absorption spectra obtained prior to dilution. Second, if the particle sizes were controlled by the concentration, then there would be a single, unique size distribution associated with any given concentration. However, this is not observed to be the case. Figure 2 shows that samples can be synthesized having comparable concentrations with size distributions ranging from reasonably monodisperse to extremely polydisperse. We find that the different size distributions are stable indefinitely.

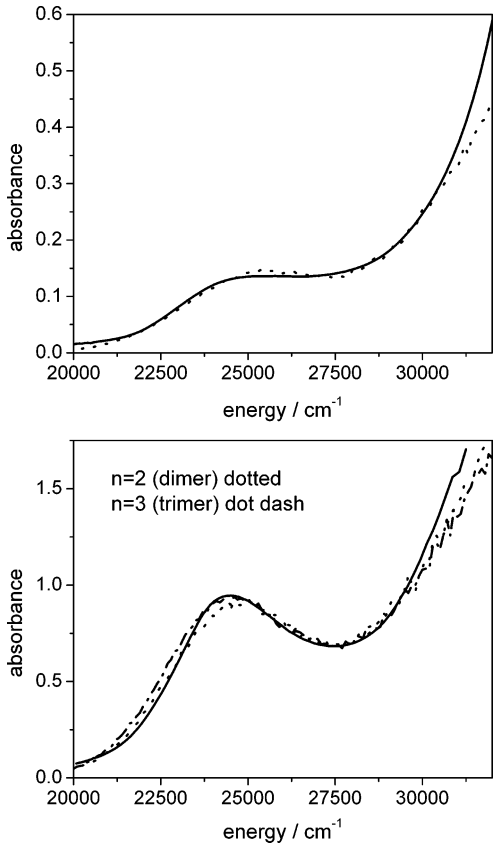

Figure 4. (A, top) Absorption spectrum of toluene-diluted sample. Also shown is a curve calculated (dotted line) with the following parameters: *z*-polarized, central energy = 25 100 cm^{-1}, width = 2000 cm^{-1}; *x*,*y*-polarized, central energy = 37 000 cm^{-1}, width = 4600 cm^{-1}, intensity ratio = 10. (B, bottom) Absorption spectrum of concentrated sample. Also shown are $n = 2$ and $n = 3$ calculated curves using the same parameters as the monomer curve and a *z*-polarized dipolar coupling of −300 cm^{-1}.

The only assignment consistent with these observations is that the spectral changes that occur at high concentrations are due to nanoparticle aggregation. The spectral changes that accompany aggregate formation are very significant and therefore suggest relatively large interactions between particles. Aggregate formation along with the presence of large interparticle interactions makes sense in terms of the known structure of the nanoparticle monomers. GaSe forms disklike nanoparticles having aspect ratios on the order of 10. The TOPO ligands are Lewis bases and are expected to bind only to the particle edges. This leaves the top and bottom selenium surfaces unligated. We will address questions of the geometry of the aggregates below. However, one would expect that at high concentrations van der Waals interactions between the nanoparticle surfaces will cause the nanoparticles to stack and thereby form aggregates.

2. Modeling of Aggregate Absorption Spectra. Figure 4 shows the absorption spectrum of a concentrated GaSe nanoparticle sample, and the same sample diluted in toluene plotted in terms of an energy (rather than wavelength) scale. Comparison of the low concentration (monomer) and high concentration (aggregate) spectra reveals two key features. First, aggregation results in a relative loss of absorbance at energies above 26 000 cm^{-1}, with this effect being most pronounced in the 26 500−29 000 cm^{-1} region. This results in the minimum in the absorption spectrum at about 27 500 cm^{-1} that is present only in the case of the aggregates. Second, the red edge of the spectrum (22 000−24 000 cm^{-1}) shifts only very slightly to the

red upon aggregation. Any reasonable model of the aggregates should be able to account for these observations.

The 20 000−32 000 cm^{-1} region of these spectra can be understood in terms of a simple model that incorporates the spectroscopy of bulk GaSe, quantum confinement effects, and dipolar coupling between the monomers. The basic ideas of this model are as follows: Bulk GaSe has a *z*-polarized transition ($\Gamma_4^- \rightarrow \Gamma_3^+$) near the band edge and an *x*,*y*-polarized transition ($\Gamma_5^- \rightarrow \Gamma_3^+$) at slightly higher energy.[34] Both of these transitions are allowed, and these two transitions are considered in this model. The above excited states are taken as zero-order monomer states. Group theory and the spectroscopy of bulk GaSe show that these two zero-order excited states interact through spin−orbit coupling.[35] The monomer eigenstates and energy levels are therefore calculated by diagonalizing a 2×2 matrix with the diagonal elements being the zero-order state energies and the off-diagonal elements being the magnitude of spin−orbit coupling. For each monomer this gives a "stick spectrum" of the two lowest transitions. Quantum confinement shifts both transitions to the blue of where they appear in bulk GaSe, and both transitions are inhomogeneously broadened. The exact position of each transition is taken randomly in an (assumed Gaussian) inhomogeneous distribution. The monomer absorption spectrum is then generated by summing many of these stick spectra, each transition sampling its Gaussian inhomogeneous distribution.

Aggregate spectra are calculated holding all of the monomer parameters constant, with the introduction of a single parameter characteristic of the aggregate, the nearest-neighbor dipolar coupling constant. For an aggregate with *n* monomers, this is done by diagonalizing a $2n \times 2n$ matrix. In the absence of interparticle coupling, this matrix is block diagonal and consists of n 2×2 monomer matrices. Other off-diagonal matrix elements are defined by the extent of dipolar coupling and the aggregate geometry. Diagonalization of this $2n \times 2n$ matrix gives the aggregate energy levels and eigenstate compositions in terms of the monomer zero-order states. The aggregate absorption spectrum is then generated by summing many of these spectra, with each of the zero-order monomer transition energies randomly sampling their inhomogeneous distributions.

The above procedure is easily applied to the case of the GaSe nanoparticle spectra in Figure 4. Both the *z*- and *x*,*y*-polarized transitions observed in bulk GaSe are shifted to the blue by quantum confinement effects in GaSe nanoparticles. A priori determination of the extents of these shifts is problematic. Electronic structure calculations have not been performed for GaSe or related types of nanoparticles. The parallel and perpendicular effective masses for lower energy transition are known and were used in our previous analysis of the size dependence of the absorption spectrum.[29] However, the exact center of the transition depends on the assumed inhomogeneous width. Furthermore, there are no determinations of the effective mass tensor for the higher energy transition. As a result, the energies of these transitions must be taken as adjustable parameters.

Inhomogeneous broadening of both bands can occur by several different mechanisms. The most obvious source of inhomogeneous broadening is the finite particle size distribution. However, qualitative considerations lead one to expect that this source of broadening may not always be the dominant source of the inhomogeneous width. In these disklike nanoparticles, quantum confinement energy shifts can be separated into *z* and *x*,*y* components. Electron diffraction and transient absorption studies indicate that the particles are one tetralayer thick, so the extent of *z*-axis quantum confinement is constant. Furthermore, previous studies have shown that in the largest particles there is little *x*,*y* quantum confinement.[29] As a result, in the most monodisperse samples, variations in particle size will have a relatively small effect on the transition energy. The above considerations can be made more quantitative. The size distribution for these samples is known from Figure 1, as is the variation of the transition energy with size (eq 1). Differentiation of eq 1 and the known standard deviation of the size distribution yields an inhomogeneous width (standard deviation) of 650 cm^{-1}. This is not negligible, but is considerably less than the observed width of the absorption onset. The conclusion is that this source of broadening cannot account for the observed width of the absorption onset and that the observed spectral width is dominated by other inhomogeneous broadening mechanisms. Probably the largest source of inhomogeneous broadening is by random surface (edge) defects. The spectrum may therefore be modeled by two inhomogeneously broadened zero-order transitions, taking their center energies, their widths, and their relative intensities as adjustable parameters. The spin−orbit interaction also affects the spectrum. The magnitude of this coupling is chosen to give the observed emission anisotropy following 410 nm excitation, about 1000 cm^{-1}. This emission anisotropy is about 0.32, indicating that about 80% of the lowest lying absorption oscillator is derived from the *z*-polarized zero-order wave function. However, with the observed emission having an anisotropy close to the limiting value of 0.4, as long as the coupling is small, the results are not very sensitive to the magnitude of this parameter.

The energies of the *z*- and *x*,*y*-polarized transitions are taken to vary independently over their inhomogeneous widths; i.e., both absorptions are taken to be delta functions and the positions of these absorptions in their (assumed Gaussian) respective inhomogeneous distributions are assumed to be uncorrelated. These assumptions are likely the least accurate approximations made in this model. The absorption spectrum of a single particle is probably not two delta functions, but has significant absorption intensity to the blue of each of the absorption onsets. This simple, delta function approximation is made because the single particle absorption spectrum is not known. The assumption that the energies of the two transitions are uncorrelated assumes that none of the inhomogeneous width is due to the finite size distribution. This is a limiting case, and we will show below that the size distribution does play some role in the observed width. Furthermore, there is no good reason to believe that the inhomogeneous energy distribution should be Gaussian. The Gaussian functional form is assumed only because it is easy to work with. With the above approximations, a calculated spectrum is obtained by summing many spectra having transition energies taken randomly from the Gaussian inhomogeneous distributions. This is a Monte Carlo approach, resulting in a small amount of noise on the calculated spectra. The results of fitting the monomer absorption spectrum are shown in Figure 4A. Despite the simplicity of the model and all of the approximations that have been made, the fit is quite good at wavelengths longer than about 310 nm. We find that the lowest energy monomer transition is characterized by a center energy and width (σ of the Gaussian) of about 25 100 and 2000 cm^{-1}, respectively. We note that this σ value relates the absorption onset (defined by the inflection in the absorption spectrum) to the actual central absorption wavelength. The higher energy transition is taken to have a central energy and width of 37 000 and 4600 cm^{-1}, respectively. Its absorption intensity is taken to be 10 times that of the lower transition. The large intensity

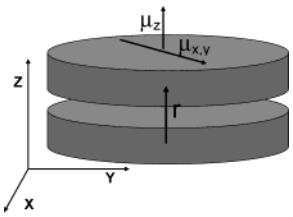

Figure 5. Schematic of the geometry and coordinate axes in a nanoparticle dimer.

ratio is not surprising. It is obvious from inspection of the absorption spectrum that the upper transition is very intense. Furthermore, XPS spectra and calculations indicate that the Γ_5^- band has a higher density of states than does the Γ_4^- band.[35−37] The parameters used to fit the higher energy transition, and to a lesser extent the lower energy transition, are not completely unique. Modest changes of positions, widths, and relative intensities can give an adequate fit to the observed spectrum. Despite this uncertainty, both transitions must have parameters that are approximately the values used to fit the spectra in Figure 3. For example, reasonable fits are obtained taking the lowest energy transition between 24 800 and 25 300 cm^{-1} and width between 1800 and 2200 cm^{-1}. Figure 4A shows that these parameters give a very good fit to the observed spectrum at energies below 32 000 cm^{-1}. We speculate that localized transitions (involving defect states) that are not considered in this simple model may become important at shorter wavelengths. Alternatively, the discrepancies at the highest energies may simply reflect the inadequacy of the assumed Gaussian inhomogeneous distribution.

The spectrum of an aggregate can be calculated by considering a system of n particles, with dipolar coupling between neighboring particles. The signs and magnitudes of the dipolar coupling terms depend on the assumed aggregate geometry. This interaction is given by

$$C_{1,2} = (\text{const}/r^3)[(\boldsymbol{\mu}_1 \cdot \boldsymbol{\mu}_2) - 3(\boldsymbol{\mu}_1 \cdot \mathbf{r})(\mathbf{r} \cdot \boldsymbol{\mu}_2)] \qquad (2)$$

where $\boldsymbol{\mu}_1$ and $\boldsymbol{\mu}_2$ are the transition dipole vectors ($\boldsymbol{\mu}_1$ and $\boldsymbol{\mu}_2$ may be either $\boldsymbol{\mu}_z$ or $\boldsymbol{\mu}_{xy}$, the z- and x,y-polarized transition dipoles), r is the dipole−dipole separation, and $\mathbf{r}$ is a unit vector between $\boldsymbol{\mu}_1$ and $\boldsymbol{\mu}_2$.[24] Because of the $1/r^3$ factor, we consider only nearest-neighbor interactions. Thus, the (const/r^3) factor is taken to be the adjustable parameter in eq 2 and this equation permits calculation of the other off-diagonal matrix elements. The orientation of $\mathbf{r}$ with respect to $\boldsymbol{\mu}_z$ and $\boldsymbol{\mu}_{xy}$ is determined by the geometry of the aggregate, and we make the most obvious assumption: that the disklike nanoparticles form stacked aggregates. In this geometry, the $\boldsymbol{\mu}_z$ or $\boldsymbol{\mu}_{xy}$ vectors are collinear and orthogonal, respectively, with the displacement vector, $\mathbf{r}$, as depicted in Figure 5. If the z-polarized dipoles point in the same direction, then this head-to-tail configuration of adjacent dipoles gives the lowest excited-state energy. Specifically, $\boldsymbol{\mu}_1 \cdot \boldsymbol{\mu}_2 = (\boldsymbol{\mu}_1 \cdot \mathbf{r})(\mathbf{r} \cdot \boldsymbol{\mu}_2) = |\boldsymbol{\mu}_z|^2$, so $C_{1,2} = -2(\text{const}/r^3)|\boldsymbol{\mu}_z|^2$. With this orientation the dipole vectors add and this state has most of the oscillator strength. In contrast, the lowest energy involving the x,y-polarized transitions corresponds to adjacent dipoles pointing in opposite directions. In this case, $\boldsymbol{\mu}_1 \cdot \boldsymbol{\mu}_2 = -|\boldsymbol{\mu}_{xy}|^2$ and $(\boldsymbol{\mu}_1 \cdot \mathbf{r})(\mathbf{r} \cdot \boldsymbol{\mu}_2) = 0$, so $C_{1,2} = -(\text{const}/r^3)|\boldsymbol{\mu}_{xy}|^2$. The vector sum of the transition dipoles is zero, and this lower energy state has no oscillator strength. All the x,y-polarized oscillator strength is in the high energy (aligned dipole) state. The conclusion is that the lower energy (z-polarized) absorption shifts to the red and the higher energy (x,y-polarized) absorption shifts to the blue upon introduction of dipolar coupling. The coupling coefficients for the z- and x,y-polarized transitions are not independent parameters. The dipolar interaction energies scale like the square of the transition dipole, as does the absorption intensity. Thus, the relative magnitudes of these couplings are related to the relative z- and x,y-polarized absorption intensities. The conclusion of the above considerations is that specifying the z-coupling coefficient and the ratio of z- and x,y-polarized absorption intensities specifies the x,y-coupling coefficient. Subsequent calculation of the n-aggregate spectrum leaves the monomer parameters unchanged and involves only a single adjustable parameter: the z-polarized dipolar coupling coefficient. With this simple model, the spectrum of an aggregate containing n monomers can be calculated. If n is taken to be large, this can be compared to the high concentration absorption spectrum. The fits to the high concentration absorption spectrum with a z-polarized coupling coefficient of -300 cm^{-1} and with $n = 2$ and 3 are shown in Figure 4B. Calculations with $n > 3$ give results very similar to those obtained with $n = 3$. Semiquantitative agreement with the experimental spectrum is obtained. This simple model explains the magnitude of the 26 000−29 500 cm^{-1} minimum in the absorption spectrum. It also predicts only a slight shift in the red edge absorption onset, in qualitative agreement with the observed result.

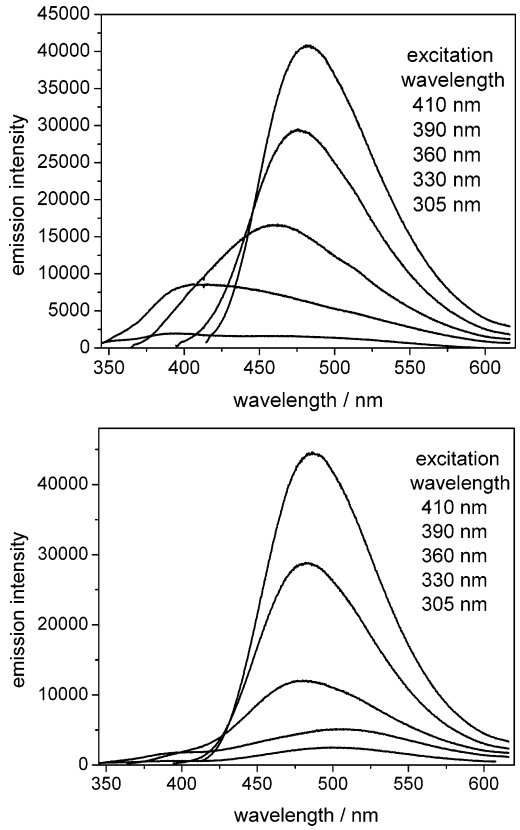

Figure 6. Emission spectra for dilute (A, top) and concentrated (B, bottom) samples following excitation at various wavelengths. The excitation wavelengths are indicated with their order reflecting the relative intensities in the 470−550 nm region. The relative intensities of the spectra have been corrected for the wavelength dependence of the excitation intensity. The sample is close to being optically thick at most of the excitation wavelengths, and the areas under the curves therefore give approximate relative emission quantum yields.

3. Emission Spectra. Emission spectra can also give considerable insight into the electronic structure of the nanoparticle monomers and aggregates. Static emission spectra, following excitation at various wavelengths, are presented in Figure 6.

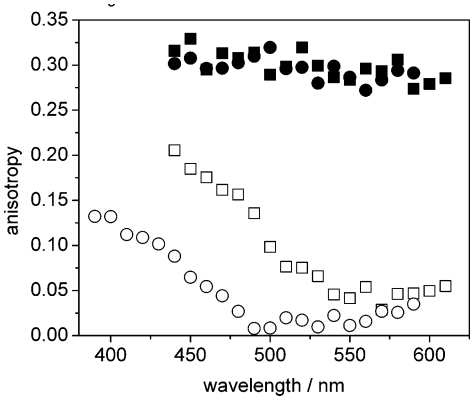

Figure 7. Initial ($t = 0$) emission anisotropy spectra for a concentrated sample following excitation at 305 nm (open circles) and 405 nm (solid circles) and for a toluene-diluted sample following excitation at 305 nm (open squares) and 405 nm (solid squares).

The emission is quite intense, with an emission quantum yield of about 15−20%. Emission anisotropy spectra are also very informative for these highly anisotropic particles. However, trapping processes can depolarize the emission, and the only easily interpreted measurements are of the emission anisotropy prior to carrier trapping. These are derived from time-resolved experiments, taking the emission anisotropy immediately following excitation. The initial ($t = 0$) anisotropy spectra, following excitation at 305 and 405 nm, are shown in Figure 7. These results are similar to and completely consistent with those previously reported.[26] Several features of these spectra are of particular interest. Following 405 nm excitation, the emission spectra of the monomers (Figure 6A) and the aggregates (Figure 6B) peak in the 480−495 nm region. In both cases, the anisotropy is quite high over the entire emission spectrum, indicating that absorption and emission are dominated by collinear oscillators. These observations confirm the most crucial part of the model proposed here: that the structure of the aggregates corresponds to a stacked geometry. The monomer emission anisotropy is about 0.33, which is close to the limiting value of 0.40 that would be obtained for collinear absorption and emission oscillators. (The reason that the observed value is slightly below 0.40 is that spin−orbit coupling mixes the *z*- and *x*,*y*-polarized transitions, as discussed above.[35,37] The magnitude of the spin−orbit coupling is set to give the experimental anisotropy following 410 nm excitation.) This large anisotropy indicates that both absorption and emission oscillators are aligned with the unique *z*-axis. It is important to note that the anisotropies for the concentrated samples are also observed to be close to 0.4. This observation indicates that, upon aggregate formation, the *z*-axes of the monomers are aligned. Other geometries would result in a lower emission anisotropy.

Further blue excitation results in weak, broad emission. For example, the emission quantum yield following 305 nm excitation is about 0.8%. The emission anisotropy spectrum (Figure 7) suggests that two distinct types of oscillators contribute to this emission. The blue edge of the spectrum exhibits a positive anisotropy, while emission red of about 475 nm is essentially unpolarized. This supports the assignment that 305 nm light primarily excites an *x*,*y*-polarized transition. Emission in the 375−450 nm range is most likely assigned to trap states that derive their oscillator strength from that *x*,*y*-polarized transition. Alternatively, some of this emission may be due to excitation of the *z*-polarized (more strongly emissive) transition of the small fraction of very small particles present in the size distribution. The TEM images (Figure 1) show very few small particles; however, the overall emission quantum yield is very small following 305 nm excitation, and it is conceivable that even a small number of strongly luminescent small particles could significantly contribute to the observed emission. In either case, this emission will have a positive anisotropy. Relaxation of the 8−9 nm particles to the lower, *z*-polarized transition results in further red emission. This relaxation results in absorption and emission dipoles that are orthogonal, and hence the lower emission anisotropy. The combination of this emission and the positive anisotropy emission from the higher lying states results in the small anisotropy observed at the longer wavelengths. Qualitatively similar results are obtained for the high concentration samples.

The calculations used to fit the absorption spectra can be used to generate calculated emission anisotropy results and thereby make the above observations somewhat more quantitative. The eigenvectors and eigenvalues that result from matrix diagonalization give the energy and composition of the absorbing state in terms of the zero-order (*z*- and *x*,*y*-polarized) monomer states. Similarly, the composition of the lowest eigenvector (corresponding to the emitting state) can also be determined. From these eigenvectors the average composition of both absorbing and emitting states and therefore the emission anisotropy may be determined, for any specified excitation wavelength. These calculated values can be compared with experimental results. Emission maxima are at about 500 nm, and the initial anisotropies at that detection wavelength are collected in Table 1. The calculated anisotropies for $n = 3$ aggregates are also given in Table 1.

The experimental results in Table 1 show that sample excitation at further blue wavelengths results in smaller anisotropies. This is easy to understand in terms of the above model. Further blue excitation excites the *x*,*y*-polarized transition, which then relaxes to the lower lying *z*-polarized state prior to emission. The calculated emission anisotropies show the same trend: further blue excitation results in smaller anisotropies. It is important to note that this qualitative agreement confirms another of the basic ideas underlying this simple model: the absorption spectrum is due to a combination of a *z*-polarized transition at lower energy and a more intense *x*,*y*-polarized transition at higher energy.

Despite predicting the correct trend, the calculated anisotropies are not quantitatively correct over the entire wavelength range. The calculation predicts smaller (negative) emission anisotropies at the furthest blue excitation wavelengths than are actually observed. This can be easily understood in terms of the assumptions and approximations made in this model. The model does not consider the possibility of emission from localized trap states. As mentioned above, emission in the 375−450 nm region is largely due to localized states that derive their oscillator strength from the *x*,*y*-polarized state and/or from a small number of strongly luminescent, very small particles. Both possibilities are ignored in the calculations, leading to only qualitative agreement with the observed anisotropy results. Furthermore, the model assumes that the *z*-polarized transition for a single particle is a delta function absorption. This is a poor approximation: the absorption surely extends to the blue. Thus, the model underpredicts the extent of *z*-polarized absorbance at the further blue wavelengths. As a result, it overpredicts the fraction of the absorbance that is *x*,*y*-polarized at the bluest excitation wavelengths and thus predicts anisotropies that are too small.

Although some aspects of this model are not quantitative, the values of the parameters needed to fit the experimental spectra give considerable insight into the nature of the inter-

TABLE 1: Emission Anisotropies Following Excitation at Various Wavelengths

excitation wavelength/nm	292	302	315	362	377	390	403	417	444
dilute	0.09	0.11	0.18	0.27	0.33	0.33	0.31	0.32	0.32
concentrated	0.022	0.048	0.11	0.27	0.31	0.33	0.33	0.32	0.33
monomer calc	−0.17	−0.17	−0.17	0.016	0.18	0.27	0.29	0.33	0.35
aggregate calc	−0.18	−0.18	−0.17	0.016	0.17	0.25	0.31	0.31	0.32

particle coupling in these aggregates. The dipolar interaction energies for both of the transitions are not very large, about −300 and 1500 cm^{-1} for the *z*- and *x*,*y*-polarized transitions, respectively. The *z*-polarized coupling is considerably less than the average difference in transition energies between adjacent nanoparticles (2000 cm^{-1}). This is why the red edge of the absorption spectrum shifts very little upon aggregate formation. In the 26 000−29 000 cm^{-1} spectral region, there is absorption from both *z*- and *x*,*y*-polarized transitions. Having a large and positive coupling coefficient, the *x*,*y*-polarized transition shifts far more to the blue than the *z*-polarized transition does to the red. The blue shift of the higher energy transition is the primary reason for the diminished absorbance in the 27 500 cm^{-1} region. The larger shift of the upper transition follows from the fact that this transition is observed to be far more intense. The presence of spin−orbit coupling also contributes to the formation of a minimum in the aggregate absorption spectrum in a way that is somewhat more subtle. Spin−orbit coupling mixes the higher and lower energy transitions, particularly in the case where the energy difference between the transitions is minimal, i.e., when the *z*- and *x*,*y*-polarized transitions are on the blue and red edges of their respective distributions. (Recall that the energies of the two transitions are taken to vary independently over their inhomogeneous distributions. This is also the most common situation with electronic transitions of organic molecules.[38,39]) As a result of this mixing, *z*-polarized transitions in this energy range shift further to the red than do those on the red edge of the absorption spectrum. This is responsible for some of the observed sharpening of the spectrum and the minimum at 27 500 cm^{-1}.

These parameters also allow us to comment on the extent to which the exciton is delocalized in these aggregates: the coherence length. A significant fraction of the aggregates have excitons that are delocalized over more than a single particle. This delocalization is responsible for the observed spectral changes. However, although significant delocalization takes place, the average coherence length is short. There is little difference between the calculated dimer and trimer spectra. This is because most of the time two adjacent particles will not have close to the same energy and having three particles in a row with close to the same energy is an unlikely event. Thus, in most cases a *z*-polarized exciton is not extensively delocalized. Examination of the eigenvalues of the aggregate calculation makes this more quantitative. The extent to which the exciton is delocalized can be characterized in terms of the fraction of the excitation (in terms of squared coefficients of the zero-order states) that is localized on a single particle. This is calculated for large ($n = 8$) aggregates. We are primarily concerned with the low energy (primarily *z*-polarized) excitons, so only energies below 27 000 cm^{-1} are considered. We find that about 46% of the excitons are more than 10% delocalized and about 29% are more than 20% delocalized. Otherwise stated, about 54% of the excitons below 27 000 cm^{-1} are at least 90% localized and 71% are at least 80% localized on a single monomer. We therefore conclude that when delocalization occurs it is usually over two, or at most a few nanoparticles.

4. Effects of Particle Size Polydispersity. The finite size distribution of the nanoparticle sample can have significant

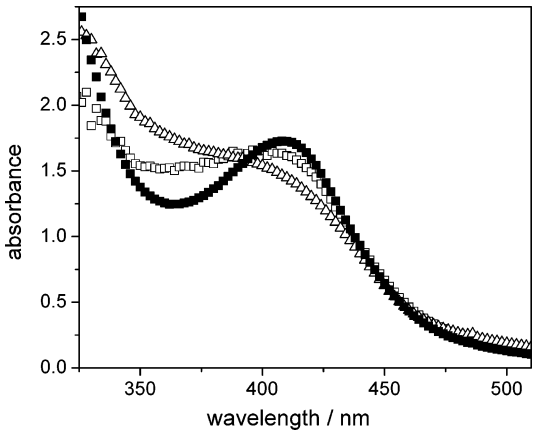

Figure 8. Absorption spectra of concentrated samples of GaSe nanoparticles in TOP/TOPO. The spectra of the monodisperse (solid squares), slightly polydisperse (open squares), and very polydisperse samples (open triangles) are shown. The spectra have been scaled to give the same absorbance at 380 nm.

effects on the absorption and especially the emission spectra. This can be seen in the emission spectra of even in the most monodisperse samples, Figure 6. In the case of the aggregates (Figure 6B), the emission maximum following 330 nm excitation is slightly to the red of that obtained following 305 nm excitation. This is because 330 nm light excites the red edge of the *x*,*y*-polarized transition and hence the largest particles; 360 nm light excites the blue edge of the *z*-polarized transition and hence the smallest particles. This size selection within each band leads to the curious observation that, while 330 nm light results in further red emission than does 305 nm light, 360 nm light results in bluer emission than either 330 or 305 nm excitation. This effect is not observed in the dilute sample (Figure 6A). This may be due to more intense blue emission in the dilute case resulting from more rapid hole trapping and/or a lack of rapid energy transfer from the smallest particles. We note that energy transfer occurs in the aggregates, and energy transfer affects the static emission spectra. However, since energy transfer can only red shift the static spectra, it does not eliminate the observed trends of the emission maxima. Energy transfer dynamics in these aggregates will be discussed in a later paper.

The effects of the size distribution are most clearly seen in the comparison of samples having very different size distributions. Figure 2 shows these effects on toluene-diluted samples. The spectra of the monodisperse and slightly polydisperse samples show a distinct shoulder at 400 nm. However, in the case of the polydisperse sample, the 400 nm shoulder is almost lost. These spectra show that, while the monodisperse samples have absorption onsets that are dominated by particle surface effects, comparable or larger broadening occurs as a result of the size distribution in polydisperse samples. Absorption spectra of the analogous concentrated samples are compared in Figure 8. As the samples become more polydisperse, the resolved peak in the 400 nm region is lost and the spectrum becomes less well resolved. Comparison of Figures 2 and 8 (specifically the monodisperse and slightly polydisperse spectra) shows that relatively small changes in the sample size distribution can result in significant changes in the aggregate spectroscopy. This

behavior is exactly what one would predict, based on the above model. The extent to which the dipolar coupling in an aggregate alters the absorption spectrum from that of the monomer depends on the fraction of nanoparticles that have an adjacent particle with close to the same transition energy; i.e., the transition energy difference is comparable to or less than the coupling energy. As the inhomogeneous width of the absorption spectrum increases, this fraction decreases, and so does the effect of aggregate formation.

5. Comparison with Organic J-Aggregates. The phenomenon of aggregation causing a red shift and sharpening of the absorption spectrum is well known for organic dye molecules, and such aggregates are referred to as "J-aggregates".[13] In such aggregates the transition dipoles are close to collinear and excitations on individual dyes interact through dipolar coupling. This results in excitons that are delocalized over some number of the monomers in the aggregate. The spectra of organic dye J-aggregates differ from the monomer spectra in two ways. First, the J-aggregate spectrum is red shifted, and the extent of this red shift is related to the extent that monomers are coupled. In the approximation that the coupling is due to the interaction of the transition dipoles, this shift may be calculated from the magnitudes of the transition dipoles and the aggregate geometry. Second, the J-aggregate spectrum is sharper and shows less vibrational structure than that of the monomer. This is because if the excitation is delocalized over many monomers, then the nuclear displacement that occurs upon photoexcitation in any one of the monomers is reduced. As a result, the extent of electron/vibration coupling is decreased and the spectrum has less intensity in transitions that change vibrational quantum numbers. Alternatively, delocalization of the exciton results in "motional narrowing" of the spectrum. Complete delocalization over a large number of monomers rarely occurs at room temperature. This is because the fluctuating thermal environment breaks the degeneracy of the individual transitions, causing some localization. The length over which the exciton is delocalized is referred to as the "coherence length". It is rarely determined by the size of the aggregate. In general, it is the extent of disorder in the aggregate that determines its coherence length. Coherence lengths in aggregates of organic dyes vary with the nature of the J-aggregate, the surrounding environment, and the temperature; values typically range from a few to a few hundred monomers.

Similar dipolar coupling interactions take place in GaSe nanoparticle aggregates, and several aspects of the aggregate spectra presented here are analogous to the spectra of J-aggregates. The biggest difference is in the magnitudes of the monomer disorder and the interparticle coupling. J-Aggregates of dyes typically have inhomogeneous widths on the order of hundreds of wavenumbers and couplings of thousands of wavenumbers. Thus, the coupling are large compared to the extent of disorder and the coherence length is quite long. The reverse is the case for the nanoparticle aggregates. The fits to the spectra indicate that the extent of disorder (the inhomogeneous line width) is greater than the interparticle coupling. As a result, the coherence length is very short.

The absorption, emission, and especially emission anisotropy results presented above have a straightforward structural interpretation: these aggregates consist of one-dimensional "stacks" of these disklike nanoparticles. As mentioned above, this is exactly the behavior one would expect from nanodisks having inert surfaces. Collapse to form bulk GaSe is prevented by the presence of the large, bulky TOP and TOPO ligands attached to the edges of the nanoparticles. In this configuration, the lowest excited state corresponds to head-to-tail interactions between individual, collinear dipoles; the spectroscopy is that of a J-aggregate. These geometric considerations highlight a fundamental difference between J-aggregates of organic dyes and these aggregates. In the case of planar, organic dyes, the transition dipoles are typically in the plane of the molecule. Thus, to get a "head-to-tail" geometry, the molecules must stack in an offset manner, rather than directly on top of each other. Molecules stacked directly on top of each other give a head-to-head geometry, resulting in a blue shift of the absorption spectrum, an "H-aggregate".[24] This is not the case for the nanoparticle aggregates, because the transition dipoles are perpendicular to the nanoparticle plane. In the *z*-polarized, nanoparticle aggregate case, linear stacking (without any offset) gives the head-to-tail geometry and is therefore analogous to organic J-aggregates despite the structural difference.

Conclusions

Several conclusions may be drawn from the results presented here.

1. GaSe nanoparticles form strongly interacting aggregates at high concentrations in room temperature solutions. The aggregate spectra are reminiscent of those of J-aggregates of organic dyes.

2. It is possible to semiquantitatively fit the monomer spectra in terms of a simple model involving the two lowest electronically excited states. The aggregate spectrum is then fit using the same parameters as for the monomer, with the inclusion of dipolar coupling between nanoparticles. The structural interpretation is that the aggregates consist of one-dimensional stacks of these disklike nanoparticles. This assignment is supported by emission anisotropy results.

3. Although a significant fraction of the excitons in the aggregates are delocalized over more than one nanoparticle, the average coherence length is short, one to two monomers. These types of aggregates are unique among semiconductor nanoparticles.

Acknowledgment. This work was supported by Grants DE-FG03-00ER15037 and DE-FG02-04ER15502 from the Department of Energy.

References and Notes

(1) Crooker, S. A.; Hollingsworth, J. A.; Tretiak, S.; Klimov, V. I. *Phys. Rev. Lett.* **2002**, *89*, 186802.
(2) Dollefeld, H.; Weller, H.; Eychmuller, A. *Nano Lett.* **2001**, *1*, 267.
(3) Dollefeld, H.; Weller, H.; Eychmuller, A. *J. Phys. Chem. B* **2002**, *106*, 5604.
(4) Micic, O. I.; Jones, K. M.; Cahill, A.; Nozik, A. J. *J. Phys. Chem. B* **1998**, *102*, 9791.
(5) Micic, O. I.; Ahrenkiel, S. P.; Nozik, A. J. *Appl. Phys. Lett.* **2001**, *78*, 4022.
(6) Kagan, C. R.; Murray, C. B.; Nirmal, M.; Bawendi, M. G. *Phys. Rev. Lett.* **1996**, *76*, 1517.
(7) Kagan, C. R.; Murray, C. B.; Bawendi, M. G. *Phys. Rev. B* **1996**, *54*, 8633.
(8) Murray, C. B.; Kagan, C. R.; Bawendi, M. G. *Science* **1995**, *270*, 1335.
(9) Leatherdale, C. A.; Bawendi, M. G. *Phys. Rev. B* **2001**, *63*, 165315.
(10) Jelly, E. E. *Nature* **1937**, *139*, 631.
(11) Scheibe, G. *Angew. Chem.* **1937**, *50*, 212.
(12) Knapp, E. W. *Chem. Phys.* **1984**, *85*, 73.
(13) van Burgel, M.; Wiersma, D. A.; Duppen, K. *J. Chem. Phys.* **1995**, *102*, 20.
(14) Fidder, H.; Knoester, J.; Wiersma, D. A. *J. Chem. Phys.* **1993**, *98*, 6564.
(15) Moll, J.; Daehne, S.; Durrant, J. R.; Wiersma, D. A. *J. Chem. Phys.* **1995**, *102*, 6362.
(16) Potma, E. O.; Wiersma, D. A. *J. Chem. Phys.* **1998**, *108*, 4894.
(17) Scheblykin, I. G.; Sliusarenko, O. Y.; Lepnev, L. S.; Vitukhnovsky, A. G.; Van der Auweraer, M. *J. Phys. Chem. B* **2000**, *104*, 10949.
(18) Spano, F. C. *J. Chem. Phys.* **2003**, *118*, 981.

(19) Spano, F. C.; Mukamel, S. *J. Chem. Phys.* **1989**, *91*, 683.
(20) Argyrakis, P.; Basko, D. M.; Drobizhev, M. A.; Lobanov, A. N.; Pimenov, A. V.; Varnavsky, O. P.; Van der Auweraer, M.; Vitukhnovsky, A. G. *Chem. Phys. Lett.* **1997**, *268*, 372.
(21) Fidder, H.; Knoester, J.; Wiersma, D. A. *J. Chem. Phys.* **1991**, *95*, 7880.
(22) Gallos, L. K.; Pimenov, A. V.; Scheblykin, I. G.; Van der Auweraer, M.; Hungerford, G.; Varnavsky, O. P.; Vitukhnovsky, A. G.; Argyrakis, P. *J. Phys. Chem. B* **2000**, *104*, 3918.
(23) Sundstrom, V.; Gillbro, T.; Gadonas, R. A.; Piskarskas, A. *J. Chem. Phys.* **1988**, *89*, 2754.
(24) Cantor, C. R.; Schimmel, P. R. *Biophysical Chemistry, Part II: Techniques for the Study of Biological Structure and Function*; W. H. Freeman: San Francisco, 1980.
(25) Levy, F. *Crystallography and Crystal Chemistry of Materials with Layered Structures*; Reidel: Dordrecht, Holland, 1976.
(26) Chikan, V.; Kelley, D. F. *Nano Lett.* **2002**, *2*, 141.
(27) Chikan, V.; Kelley, D. F. *J. Chem. Phys.* **2002**, *117*, 8944.
(28) Chikan, V.; Kelley, D. F. *Nano Lett.* **2002**, *2*, 1015.
(29) Tu, H.; Chikan, V.; Kelley, D. F. *J. Phys. Chem. B* **2003**, *107*, 10389.
(30) Peng, X.; Wickham, J.; Alivisatos, A. P. *J. Am. Chem. Soc.* **1998**, *120*, 5343.
(31) Chikan, V.; Kelley, D. F. *J. Phys. Chem. B* **2002**, *106*, 3794.
(32) Lin, X. M.; Wang, G. M.; Sorenson, C. M.; Klabunde, K. J. *J. Phys. Chem. B* **1999**, *103*, 5488.
(33) Lim, X. M.; Sorenson, C. M.; Klabunde, K. J. *J. Nanoparticle Res.* **2000**, *2*, 157.
(34) Mooser, E.; Schluter, M. *Nuovo Cimento* **1973**, *18B*, 164.
(35) Schluter, M. *Nuovo Cimento* **1973**, *13B*, 313.
(36) Camara, M. O. D.; Mauger, A.; Devos, I. *Phys. Rev. B* **2002**, *65*, 125206.
(37) Schlüter, M.; Camassel, J.; Kohn, S.; Voitchovsky, J. P.; Shen, Y. R.; Cohen, M. L. *Phys. Rev. B* **1976**, *13*, 3534−3547.
(38) Griesser, H. J.; Wild, U. P. *J. Chem. Phys.* **1980**, *73*, 4715.
(39) Lee, H. W. H.; Walsh, C. A.; Fayer, M. D. *J. Chem. Phys.* **1985**, *82*, 3948.